



ELSEVIER

Deep-Sea Research II 52 (2005) 1684–1704

DEEP-SEA RESEARCH
PART II

www.elsevier.com/locate/dsr2

A tracer study of ventilation in the Japan/East Sea

C.F. Postlethwaite^{a,b,*}, E.J. Rohling^a, W.J. Jenkins^{a,c}, C.F. Walker^a

^a*School of Ocean and Earth Science, University of Southampton, National Oceanography Centre, Southampton SO14 3ZH, UK*

^b*Proudman Oceanographic Laboratory, 6 Brownlow Street, Liverpool L3 5DA, UK*

^c*Woods Hole Oceanographic Institution, Woods Hole, MA 02543, USA*

Received 14 September 2002; received in revised form 23 June 2004; accepted 22 July 2004

Abstract

During the Circulation Research in East Asian Marginal Seas (CREAMS) summer cruises in 1999, a suite of samples was collected for tracer analysis. Oxygen isotopes combined with tritium-helium ventilation timescales and noble gas measurements give unique insights into the ventilation of water masses in the Japan/East Sea (JES). In particular, noble gases and oxygen isotopes are indicators of brine rejection, which may assist in explaining the recent changes observed in the ventilation of the JES. Oxygen isotope data presented here indicate that both thermally driven convection and brine rejection have played significant roles in deep-water formation but that brine rejection is unlikely to be a significant contributor at the moment. A 6-box ventilation model of the JES, calibrated with tritium and helium-3 measurements, performed better when a significant decrease of dense-water formation rates in the mid-1960s was incorporated. However, the model calculations suggest that Japan Sea Intermediate Water formation is still occurring. Subduction of sea-ice melt water may be a significant ventilation mechanism for this water mass, based on an argon saturation minimum at the recently ventilated salinity minimum in the northwestern sector of the JES. The salinity and oxygen isotope budgets imply a potential bottom-water formation rate of $3.97 \pm 0.89 \times 10^{12} \text{ m}^3 \text{ yr}^{-1}$ due to brine rejection, which could account for a time averaged fraction of between 25% and 35% of the ventilation of subsurface water formation in the JES.

© 2005 Elsevier Ltd. All rights reserved.

1. Introduction

Over the past 50 years, the potential temperature of the deep and bottom waters of the Japan/East Sea (JES) has increased, while dissolved oxygen concentrations have decreased, suggesting

climatic shifts in the formation and ventilation rates of these water masses (Gamo and Horibe, 1983; Gamo et al., 1986; Kim and Kim, 1996; Kim et al., 2001). There has been much speculation regarding the changing contributions of the various ventilation mechanisms responsible for these changes. Although dissolved oxygen, carbon-14 and tritium profiles indicate that deep convection occurs within the JES (Gamo and Horibe, 1983; Watanabe et al., 1991), it was only

*Corresponding author. Tel.: +44 151 7954800;
fax: +44 151 7954801.

E-mail address: cfpo@pol.ac.uk (C.F. Postlethwaite).

in the winter of 2000–2001 that this convection was actually recorded relatively soon after it occurred (Kim et al., 2002; Talley et al., 2003). It remains unclear whether these convective events were driven by brine rejection or buoyancy loss by cooling because the resultant T-S signature is ambiguous, and water mass properties within the JES are relatively homogeneous. In other words, the enhanced salinity observed in the convecting water could have originated either from a more saline water mass (for example, an eddy of warm salty subtropical water shed from the sub-polar front) by excessive latent-heat extraction, or from brine rejection processes. Here, we employ additional conservative tracers such as oxygen isotope ratios and noble gas abundances to help distinguish between these different mechanisms, using samples from cruises in the JES during July and August 1999.

2. Methods

2.1. Sampling

Fig. 1 is a map of the hydrographic and tracer station locations of the Circulation Research in East Asian Marginal Seas (CREAMS) summer cruises of 1999 superimposed on the bottom topography of the JES. Samples for tracer studies were collected with R.V. *Roger Revelle* of the Scripps Oceanographic Institution (San Diego) and R.V. *Professor Khromov* of the Pacific Oceanological Institute (Vladivostok). A total of 158 samples from 22 stations were analysed for oxygen isotopes, 136 samples from 18 stations were analysed for noble gas abundances and helium isotopes, and 293 samples from 37 stations were analysed for tritium, with 12–19 samples per station for stations with depths greater than 1000 m.

2.2. Analytical procedures

Water samples for noble gas analysis were collected from Niskin bottles in cold-welded copper tubing. The gases were vacuum extracted from the water samples into aluminosilicate glass

ampoules and analysed at the Southampton University Noble Gas Laboratory by mass spectrometric peak-height manometry using automated techniques described by Lott and Jenkins (1984). Measurements were made to an accuracy of 0.8% for He, in a magnetic-sector mass spectrometer, and to 1.1% for Ne, and 1.2% for Ar in a quadrupole mass spectrometer. The results were corrected for processing blanks and extraction efficiencies by an amount generally less than measurement precision. Helium isotope ratio measurements were made relative to atmospheric helium standards, to an accuracy of 0.25%, and were corrected for instrumental linearity, which was determined by measurement of differing-sized air standards. Helium isotope data are reported as isotope ratio anomalies relative to an atmospheric standard, which is defined in the usual manner by

$$\delta^3\text{He} = \left(\frac{[{}^3\text{He}/{}^4\text{He}]_X}{[{}^3\text{He}/{}^4\text{He}]_{\text{Air}}} - 1 \right) \times 100\%.$$

Samples for tritium analysis were collected in pretreated argon-filled 1-litre glass bottles sealed with polycone-lined lids. Tritium is reported in Tritium Units (T.U.) defined as the isotopic ratio ${}^3\text{H}/{}^1\text{H}$ multiplied by 10^{18} . Tritium was measured by the helium-3 ingrowth technique at the University of Southampton Noble Gas Laboratory (Clarke et al., 1976) to an accuracy of 1.2% and a detection limit of 0.001TU. Samples for oxygen isotope analysis were collected in 250-ml glass bottles that had been pre-treated in the same way as those for tritium analysis. These samples were analysed on the Southampton Oceanography Centre VG903 manual mass spectrometer with 24-vial equilibration front line, and are reported relative to the VSMOW standard using

$$\delta^{18}\text{O} = \left(\frac{[{}^{18}\text{O}/{}^{16}\text{O}]_X}{[{}^{18}\text{O}/{}^{16}\text{O}]_{\text{VSMOW}}} - 1 \right) \times 1000\%.$$

External precision was $\sim 0.05\%$.

Salinity and temperature results presented here are from the bottle data collected during the 1999 CREAMS summer cruises (L. Talley, Pers. Commun., N.O.D.C.)

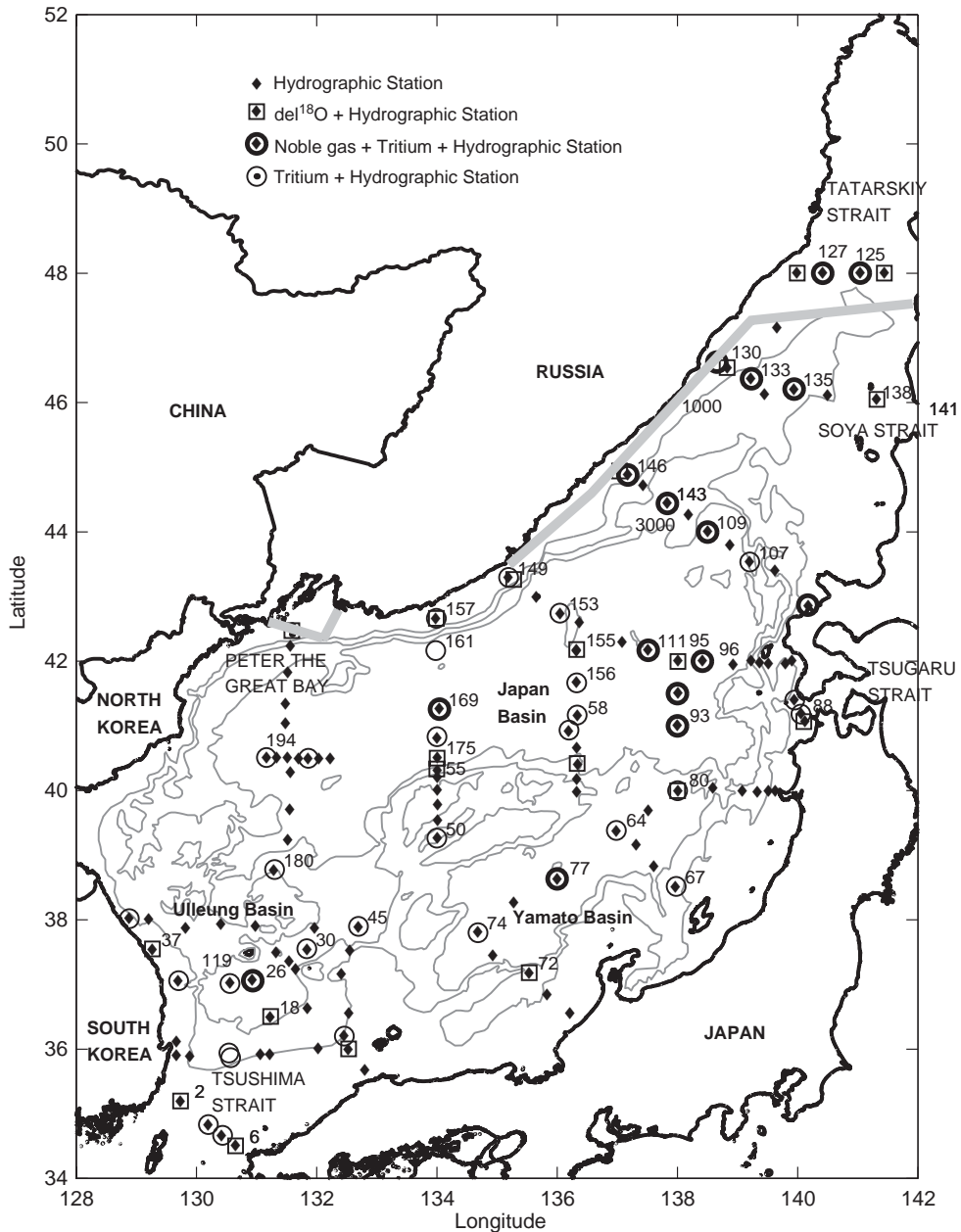


Fig. 1. Hydrographic and tracer station locations for the 1999 CREAMS summer cruises overlaid on the bathymetry of the JES. The thick grey line shows the approximate maximum sea-ice extent during the winter preceding the cruise (National Ice Centre, Washington DC).

3. Results

3.1. Oxygen isotopes

Surface temperature and salinity data have been contoured (Figs. 2a and b) and overlain with

surface $\delta^{18}\text{O}$ values. Salinity and $\delta^{18}\text{O}$ are highly correlated in the surface waters of the JES (Fig. 3), meaning that a contour plot of surface salinity (Fig. 2a) can act as a visualization tool for the surface distribution of $\delta^{18}\text{O}$, which is otherwise too

sparse to contour on the same scale as salinity. A clear regional contrast exists between positive $\delta^{18}\text{O}$, high-salinity waters in the south and east of the JES and negative $\delta^{18}\text{O}$, low-salinity waters in the north–northwestern sector. The isotopically heavy water mass in the south corresponds to the salty Tsushima Warm Current. The average $\delta^{18}\text{O}$ value for samples from all depths within the Tsushima Strait (stations 2 and 6) is $0.33 \pm 0.07\%$. Surface samples warmer than 16°C (dots, Fig. 3) form a clear linear relationship between $\delta^{18}\text{O}$ and salinity (called Warm Mixing Line, Fig. 3, $\delta^{18}\text{O} = -13.8(\pm 1.5) + 0.41\text{S}$, $r^2 = 0.93$), with end members north of the sub-polar front and the Tsushima Warm Current.

Waters in the northern JES appear isotopically light. $\delta^{18}\text{O}$ values in the Liman Current, which is characterized by the narrow band of low-salinity water running southwards along the Russian Coast, are among the isotopically lightest observed during this survey. Surface samples that are colder

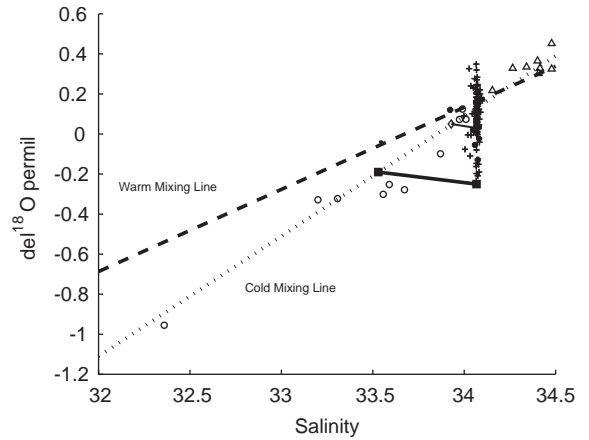


Fig. 3. $\delta^{18}\text{O}$ plotted against salinity. Triangles are data from the Tsushima Strait region (stations 2 and 6), dots are from surface water warmer than 16°C , open circles are from surface water colder than 16°C and crosses are from the subsurface water masses from all other regions of the JES. The diamonds and squares indicate the change in salinity and $\delta^{18}\text{O}$ brought about by brine rejection caused by 0.6% and 2% of the mixed-layer freezing, respectively.

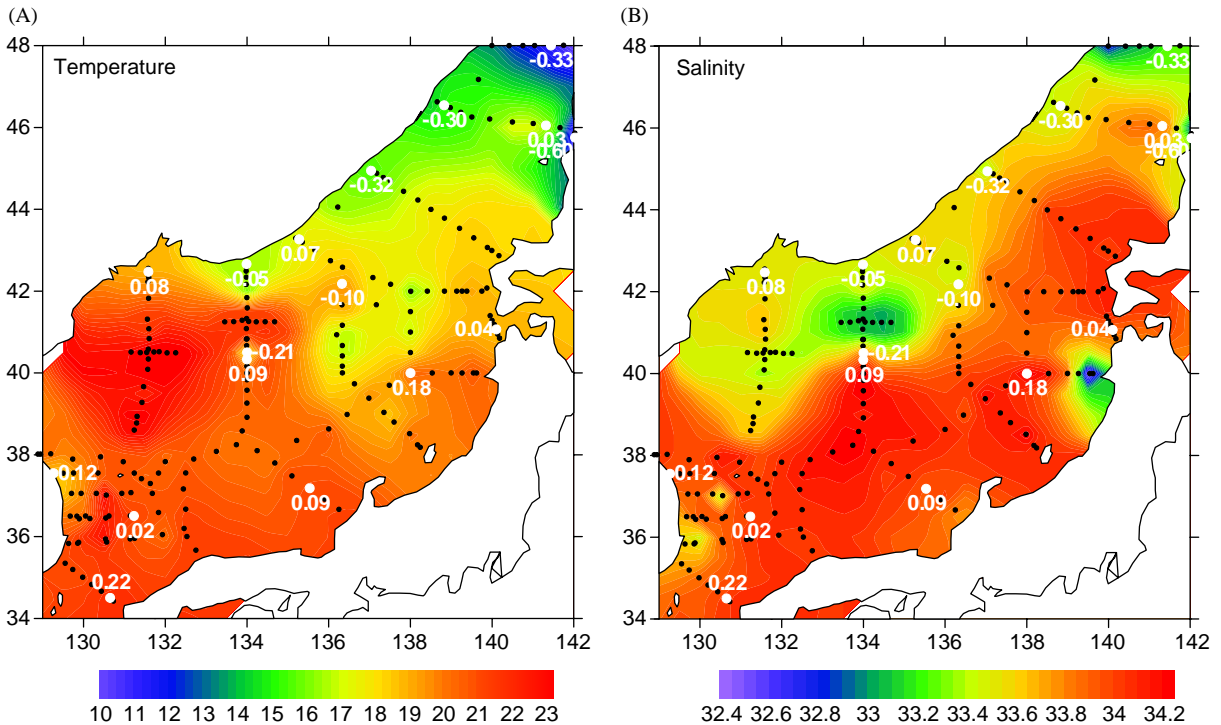


Fig. 2. Contour plots of (A) sea-surface temperature ($^\circ\text{C}$) and (B) sea-surface salinity. Black dots indicate the station location of hydrographic stations and white dots indicate the location of surface oxygen isotope measurements. The oxygen isotope values are shown in white.

than 16 °C, within the region influenced by the Liman Current and the Soya Strait, do not fall on the warm-water mixing line, but are shifted towards isotopically lighter values (called Cold Mixing Line, Fig. 3, $\delta^{18}\text{O} = -20.31 (\pm 1.8) + 0.60\text{S}$, $r^2 = 0.97$). Although we are unaware of any direct measurements of $\delta^{18}\text{O}$ in the Amur River that flows into the northern Tatarskiy Strait, precipitation measurements from similar latitudes to the Amur, suggest a freshwater end member of approximately -15‰ (Yamamoto et al., 2001). The significantly more negative intercept of the Cold Mixing Line is consistent with the hypothesis (Martin and Kawase, 1998) that brine-rejection mechanisms associated with seasonal sea-ice formation and melting within the Tatarskiy Strait may play a significant role in the formation of the Liman Current.

Subsurface samples form a cluster of points with a relatively uniform salinity of approximately 34 but with a wide spectrum of $\delta^{18}\text{O}$ values (-0.25 to 0.35). The range of $\delta^{18}\text{O}$ found in the subsurface water masses is nearly as wide as that found in the surface, whereas the salinity, which influences buoyancy, is an order of magnitude less variable. This suggests that the subsurface water masses achieve their densities through a variety of mechanisms.

3.2. Dissolved noble gases

In general, the dissolved light noble gas concentrations (helium, neon and argon) show a minimum at the surface and increase towards the bottom (Figs. 4b–d). Argon is up to 6% supersaturated compared to equilibrium with the atmosphere in the surface waters due to radiative warming (Fig. 5b), consistent with the fact that in the spring and summer the near-surface layers are heated faster than argon can be lost by gas exchange to the atmosphere (see Spitzer and Jenkins, 1989). Stratification further serves to inhibit vertical mixing, thereby trapping these supersaturations in subsurface waters. In waters below the 10 °C isotherm argon is undersaturated due to the effects of winter cooling, whereby heat extraction occurs faster than argon uptake from the atmosphere. Dissolved oxygen also switches from supersaturation to

undersaturation at this isotherm. Biological oxygen production and utilization causes the oxygen saturation anomalies to be greater than those for argon (Figs. 4a, b and 5b). Helium and neon are supersaturated throughout the water column and the saturation anomalies show no apparent temperature dependence (Figs. 5c and d). Heating and cooling are less important for helium and neon, whose solubility and temperature dependence are so low that air injection becomes a more dominant process (Spitzer and Jenkins, 1989).

The imprint of ventilation mechanisms on noble gas concentrations may be more pronounced in subsurface waters where gas exchange with the atmosphere is inhibited. Argon concentration vs. helium concentration plots can provide insight into the relative importance of sea-ice formation and thermal convection to deep-water ventilation. Fig. 6 shows argon concentration plotted against helium concentration with density indicated by the colour of the symbols on the plot. The low-density surface water gas concentrations follow an approximately linear trend governed by the respective temperature-solubility dependences of the gases. A cluster of denser water samples (top right corner Fig. 6) shows concomitant increases in argon and helium concentrations, along an argon:helium ratio trend indicative of air injection/addition. These samples appear to be affected by open-ocean convection, as the wind and wave action associated with this process can lead to the injection of bubbles into the convecting water mass. (e.g., see Wallace and Wirick, 1992; Keeling, 1993). Another group of samples (top left corner Fig. 6) shows increased argon concentrations coupled with decreased helium concentrations, which is consistent with that expected from sea-ice formation and brine rejection, since helium is relatively soluble in sea ice while argon is not (Hood et al., 1998; Postlethwaite, 2002). The latter group exclusively concerns stations from the western Japan Basin and the western Tatarskiy Strait.

3.3. Tritium and helium-3

Tritium (^3H) profiles for representative stations in the JES are shown in Fig. 7a. ^3H is usually

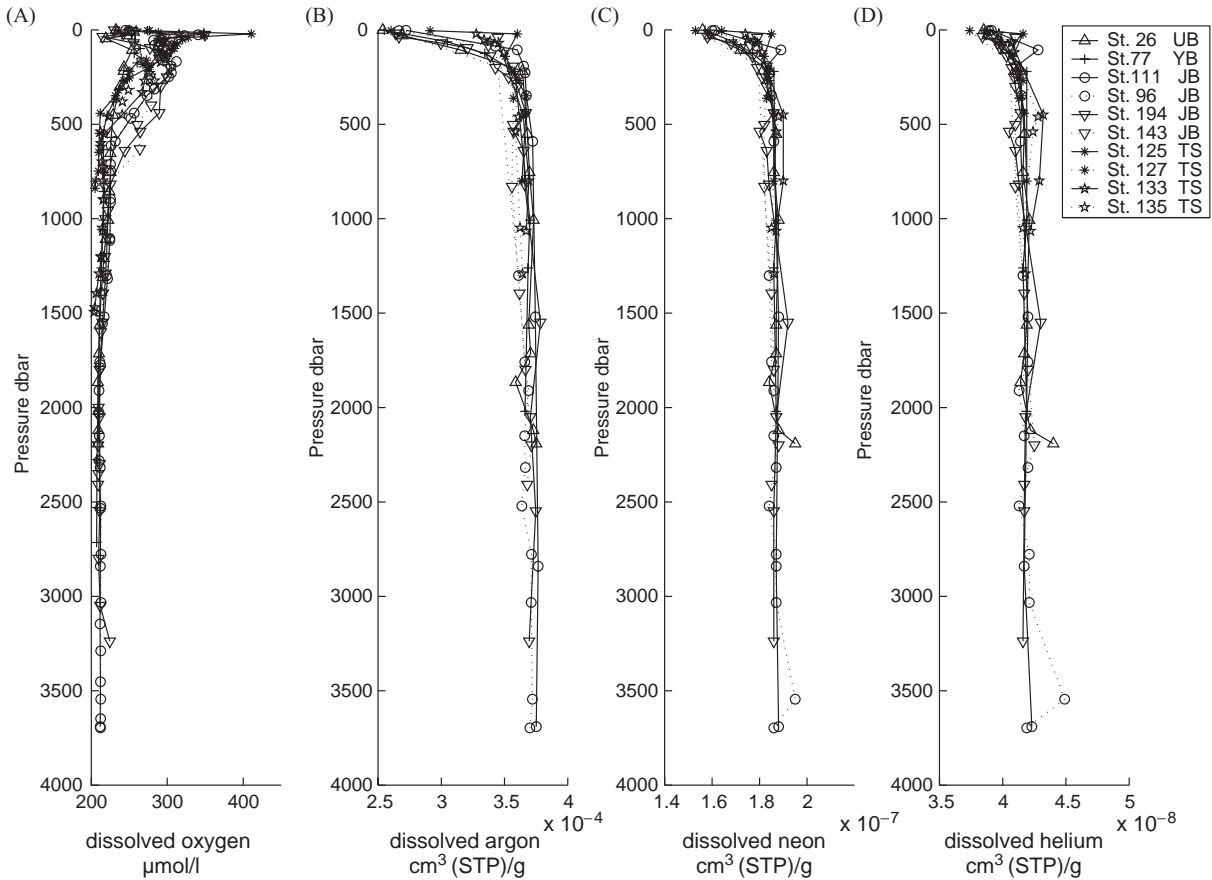


Fig. 4. Profiles of dissolved oxygen, dissolved argon, dissolved neon and dissolved helium concentrations for stations in the JES. (UB = Ulleung Basin, YB = Yamato Basin, JB = Japan Basin, TS = Tatarskiy Strait).

greatest at the surface with values between 1.5 and 2 TU. From the surface, tritium decreases nearly monotonically to around 0.5 TU at about 1500 m. There is then an exponential decrease to about 2500 m beneath which tritium is homogeneous. In their 1987 tritium observations in the JES, Watanabe et al. (1991) observed a mean concentration of 0.6 TU99 (TU decay corrected to January 1999) in the water column beneath 200 m depth and 1.9 TU99 in the surface 200 m. At two of their stations they observed tritium concentrations slightly above analytical error (0.16 TU99) at a depth of 2000 m, which they considered evidence of rapid vertical mixing relative to the northwest Pacific. The mean concentration observed in the surface 200 m from our 1999

CREAMS samples is 1.56 TU99, a significant decrease in surface ^3H concentration during the intervening time period due to a combination of decreasing atmospheric deposition (S. Stark, Pers. Commun.) and removal of ^3H from the surface to deeper waters by convection.

The Tsushima Warm Current is seen as a tritium minimum just below the surface in stations from the Ulleung and Western Japan Basins (Fig. 7a). This minimum reflects the origin of this current from the subtropical Kuroshio where the atmospheric deposition of tritium is relatively lower (Broecker et al., 1986; Stark et al., 2004). The highest tritium values of around 2.1 TU99 are found in surface waters in the Tatarskiy Strait (stations 125 and 127).

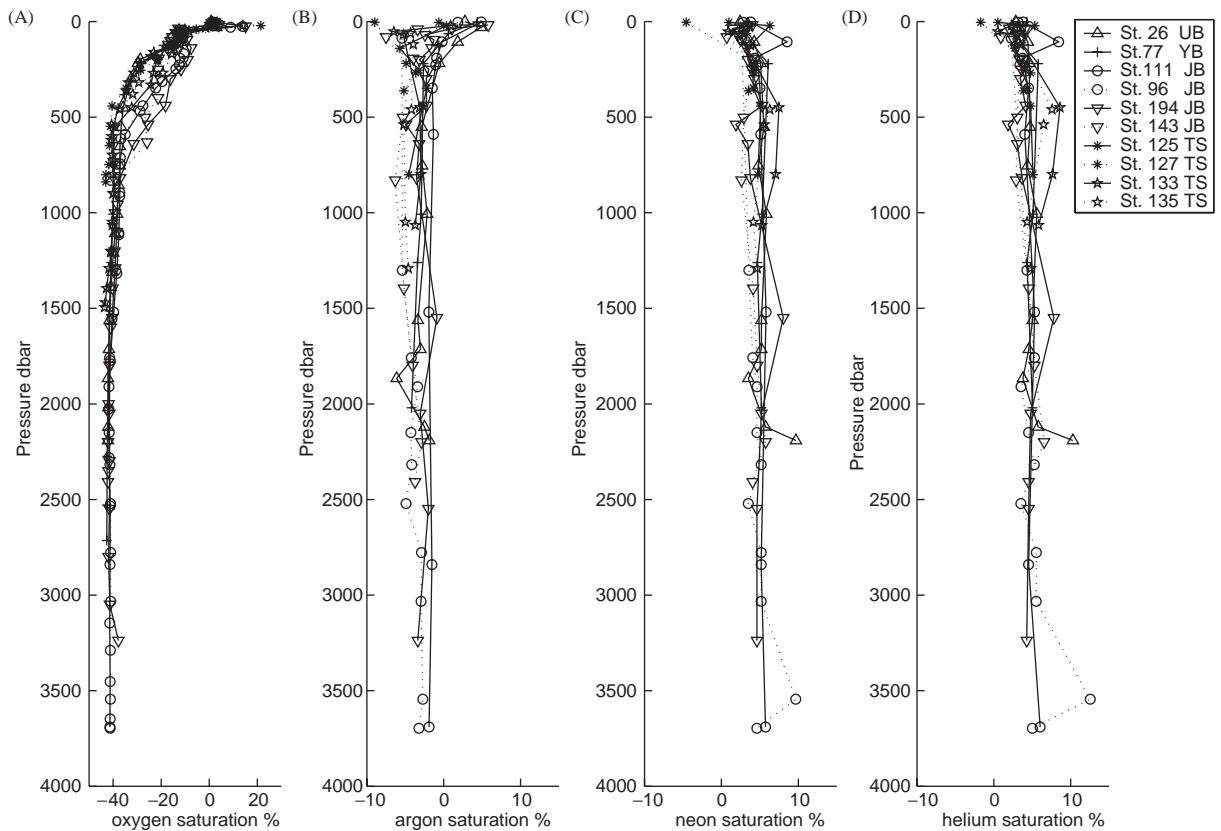


Fig. 5. Profiles of oxygen, argon, neon and helium saturation anomalies for stations in the JES. (UB = Ulleung Basin, YB = Yamato Basin, JB = Japan Basin, TS = Tatarskiy Strait).

There appear to be spatial differences in tritium distribution for depths between 200 and 1500 m, with the lowest values found in the Tatarskiy Strait and increasing towards the south (Fig. 7a). This is consistent with observations of increasing dissolved O_2 and CFC concentrations towards the south (Riser et al., 1999), which was attributed to a southward deepening of isopycnals. Samples from greater than 1000 m depth are plotted against σ_2 in Fig. 7b. Surprisingly, for any given density horizon, the tritium concentrations in the Tatarskiy Strait are up to 0.2 TU lower than in the rest of the Japan Sea. This is thought to be a region of deep-water ventilation by brine rejection (e.g. Martin et al., 1992) and although ice formation involves isotopic fractionation, with the heavier isotope (i.e. tritium) accumulating in the ice and resulting in tritium depleted brine, this effect

would be far too small to generate the low tritium values described here. We propose that the depressed tritium values in the Tatarskiy Strait indicate older water, which would suggest that brine rejection in that region is not currently an important process in deep-water ventilation, or that the transport of freshly ventilated water masses occurs via deep boundary currents, not represented by the station shown here.

For densities greater than $\sigma_2 = 36.67 \text{ kg/m}^3$ tritium concentrations converge in the three main basins of the JES, although tritium continues to decrease with increasing density. The mean bottom-water tritium concentration is 0.13 TU99, or about 100 times larger than our detection limit. This concentration is significantly greater than comparable depths in the open North Pacific, suggesting that vertical mixing or deep-water

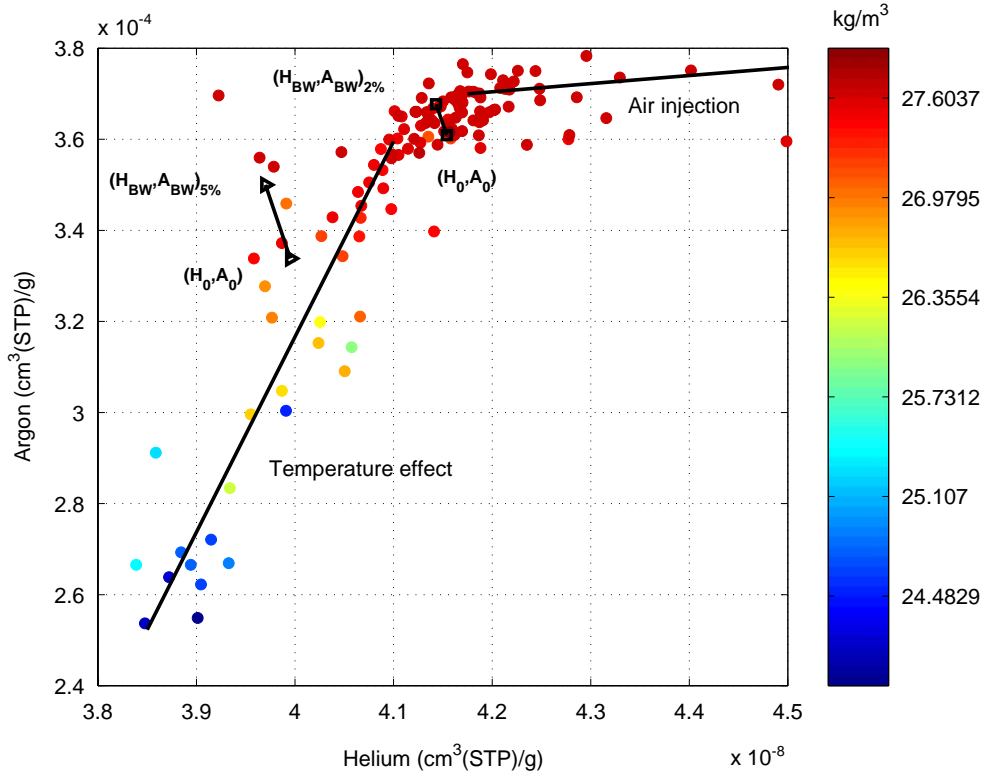


Fig. 6. Argon concentration plotted against helium concentration. The colour of the symbols indicates σ_0 (kg/m^3), the density of the samples referenced to the surface. The black lines indicate the effect of increasing temperature on helium and argon solubility and the impact of complete dissolution of air at atmospheric ratios on helium and argon concentration.

formation processes have actively modified water mass properties in this basin during the latter half of the 20th century.

The summary plot of $\delta^3\text{He}$ profiles (Fig. 8a) shows that $\delta^3\text{He}$ is close to solubility equilibrium near to the surface ($\sim -1.7\%$; Benson and Kraus, 1980) and increases downward into the water column. In the western Japan Basin a low $\delta^3\text{He}$ interval exists between 200 and 500 m (Fig. 8a). A $\delta^3\text{He}$ maximum of approximately 8% is found between 500 and 1000 m, reflecting the vertical propagation of the tritium input spike and the ingrowth of its daughter isotope, ^3He . Below 1000 m, $\delta^3\text{He}$ decreases to about 2% between 2500 and 3500 m. Here $\delta^3\text{He}$ is rather homogeneous.

The $\delta^3\text{He}$ data show differences between the various basins in the deeper waters of the JES (Fig. 8b), which contrasts with the relatively homo-

geneous tritium concentrations for these water masses (Fig. 7b). $\delta^3\text{He}$ in the Ulleung Basin is approximately 1% higher than in the Japan Basin for $\sigma_2 > 36.67 \text{ kg/m}^3$, which corresponds to a tracer age difference of approximately 5 years between these basins in the JES. No samples from the Tatarskiy Strait region match these densities.

4. Discussion

4.1. A multi-box ventilation model of the JES

Several studies have looked at quantifying the changes that have occurred in the JES by means of simple box models of chemical tracers such as ^{14}C (Gamo and Horibe, 1983, Kumamoto et al., 1998), Ra-226 (Harada and Tsunogai, 1986), CFCs (Min,

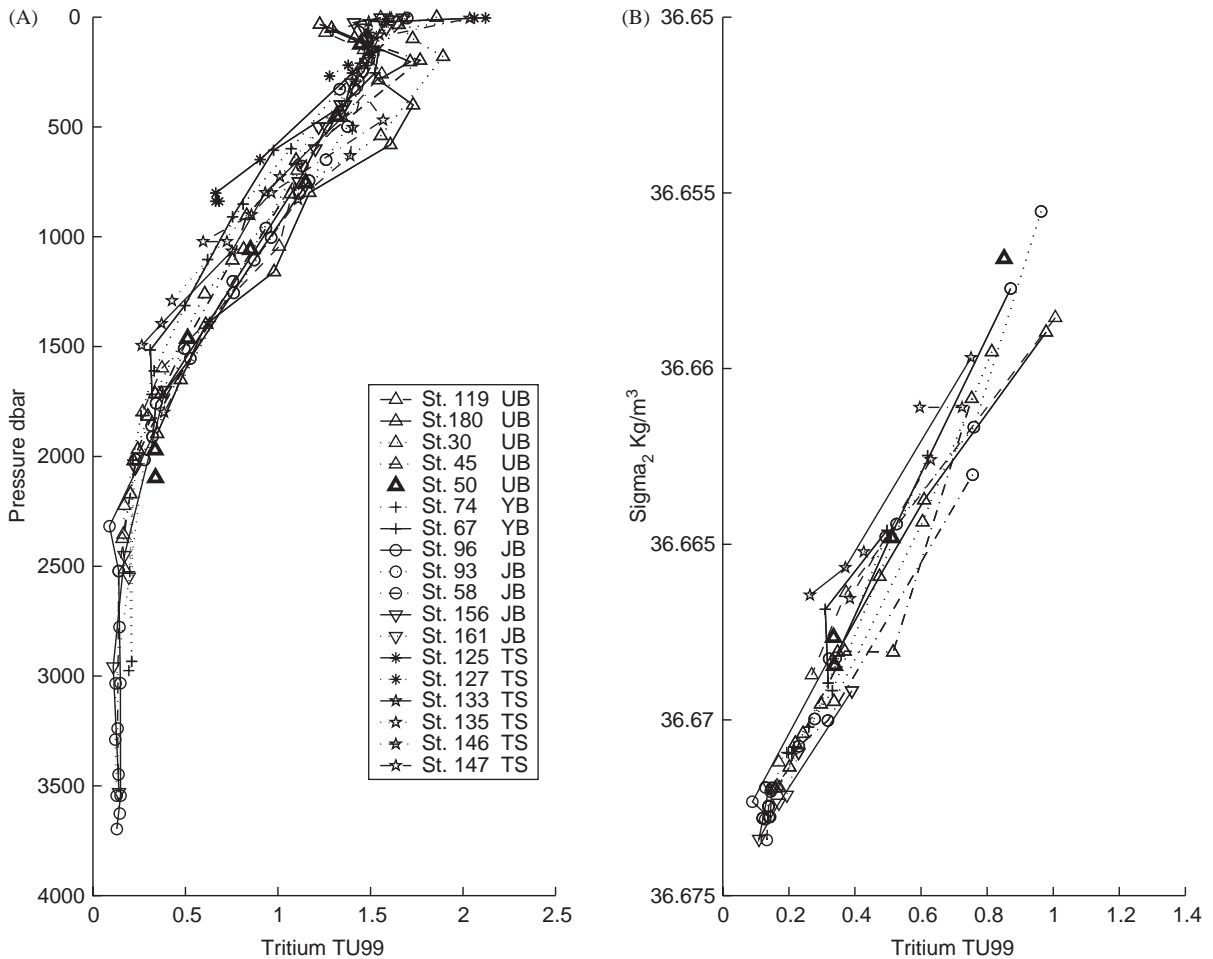


Fig. 7. (A) Depth profiles of tritium (TU99) for stations in the JES and (B) density profiles (σ_2 , kg/m³) of tritium (TU99) for samples from greater than 1000 m. (UB = Ulleung Basin, YB = Yamato Basin, JB = Japan Basin, TS = Tatarskiy Strait).

1999; Riser et al., 1999) and tritium (Watanabe et al., 1991; Kim, 1997). These range from very simple two-box steady-state models to more complex models with moving boundaries that attempt to capture the characteristics of the changing water mass structure within the JES over the past few decades. The residence time of the JES bottom water calculated from these models vary from as little as 75 years (Kumamoto et al., 1998) to as much as 500 years (Riser et al., 1999). Many of these models have been calibrated with data from a single point in time, as time-series data for these chemical tracers have not been available.

4.1.1. Model description

Here we construct a 6-box model to represent the major water masses of the JES (see Fig. 9), and optimise the various exchange and water mass formation rates against available observations of tritium and ³He. The surface layer of the JES, representing the top 200 m, is divided into two equal sized boxes, a southern and northern box divided by a sub-polar front. Subsurface boxes consisting of Intermediate Water (200–600 m depth), Central Water (600–1500 m depth), Deep Water (1500–2500 m depth) and Bottom Water (>2500 m depth) constitute the remaining boxes.

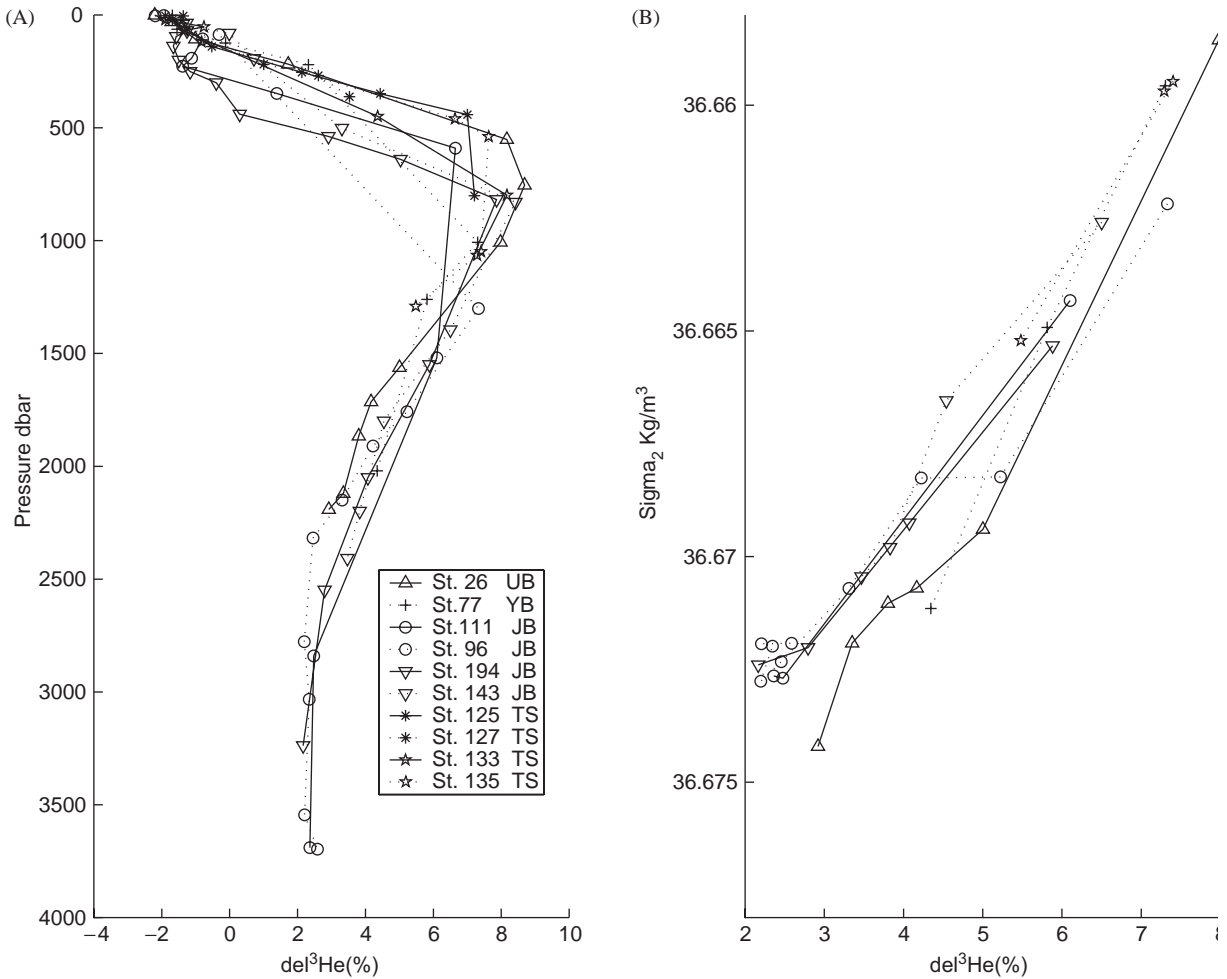


Fig. 8. (A) Depth profiles of helium-3 for stations in the JES and (B) density profiles (σ_2 , kg/m^3) of helium-3 for samples from greater than 1000 m. (UB = Ulleung Basin, YB = Yamato Basin, JB = Japan Basin, TS = Tatarskiy Strait).

The volume of each box, based on the hypsometry of Menard and Smith (1966), is shown in units of 10^{12} m^3 in the lower left hand corner of each box in Fig. 9.

Flow through each of the straits is specified from various other studies, and unlabeled inter-box flows are computed to conserve mass (e.g., upwelling return flow from the water mass formation flux). The flux through the Tatarskiy Strait consists of a fraction of the Amur River outflow and the flux through the Tsushima Strait originates from the sub-tropical North Pacific.

Atmospheric deposition was computed separately for Southern and Northern surface boxes using individual tritium in precipitation curves obtained from a reanalysis of the IAEA data set (Fig. 10(a), from Stark et al., 2004) combined with the SOC climatology for precipitation, evaporation and humidity (Josey et al., 1999) and the appropriate equation (Doney et al., 1993). The time series of tritium in the sub-tropical North Pacific (Fig. 10(b)) for inflow through the Tsushima Strait, and in the Amur River (Fig. 10(c)) for inflow through the Tatarskiy Strait are derived

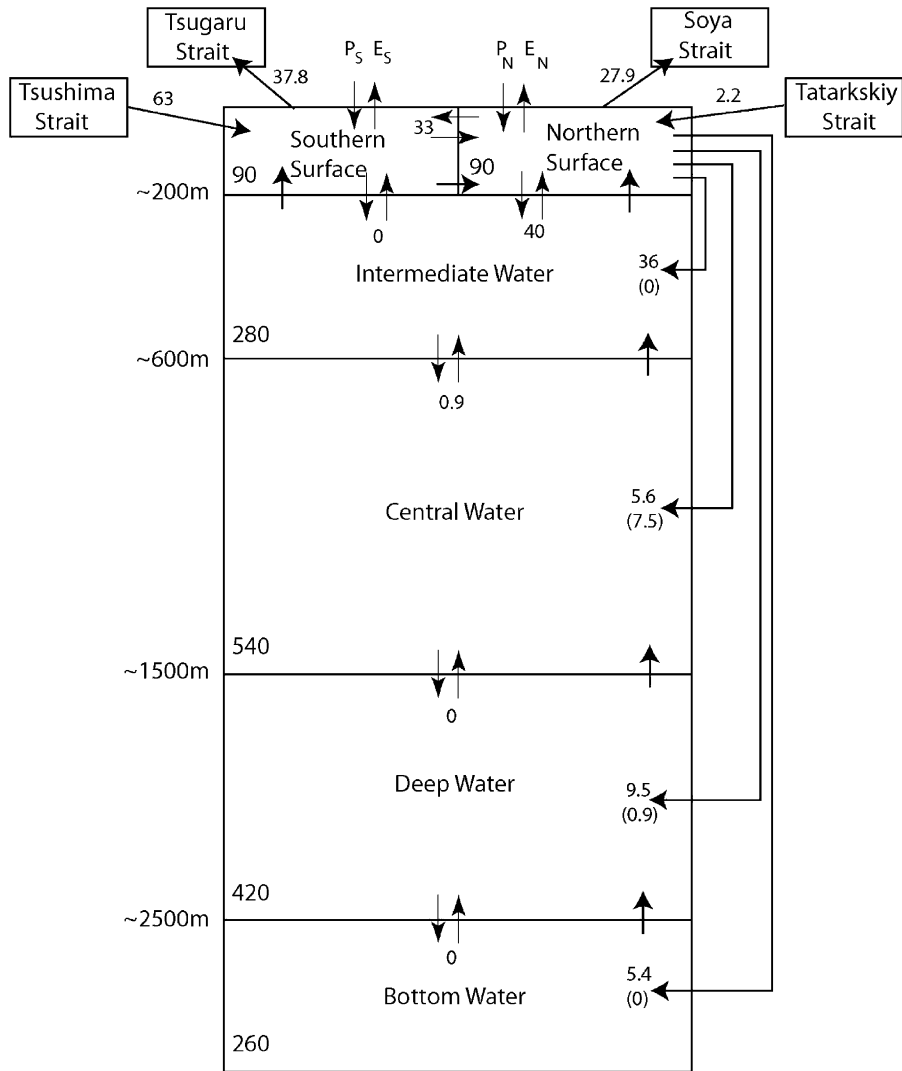


Fig. 9. The 6-box ventilation model of the JES with boundary conditions and interior processes. Volumes in the lower left-hand corner of each box are in units of 10^{12} m^3 , and labelled arrows are in units of $10^{12} \text{ m}^3 \text{ yr}^{-1}$. Double arrows indicate exchange, and unlabelled arrows indicate one-way flows necessary for flow closure. Numbered arrows are results from the optimised non-steady state model with the post 1966 fluxes in parentheses.

from a North Pacific tritium model constrained by GEOSECS and WOCE observations (Stark et al., 2004).

Exchange fluxes between the boxes (the six double arrow pairs at each interface) are treated as adjustable parameters as are the water mass formation rates (the four vertical arrows extending downward between the northern surface box and

the subsurface boxes on the right of Fig. 9). Upwelling flows (the five vertical arrows) and the surface northward flow are computed to conserve mass. The return flow from the bottom, deep, and central boxes is split equally between the southern and northern surface boxes, and the intermediate formation flows into the southern surface box only. The northward surface flow balances mass

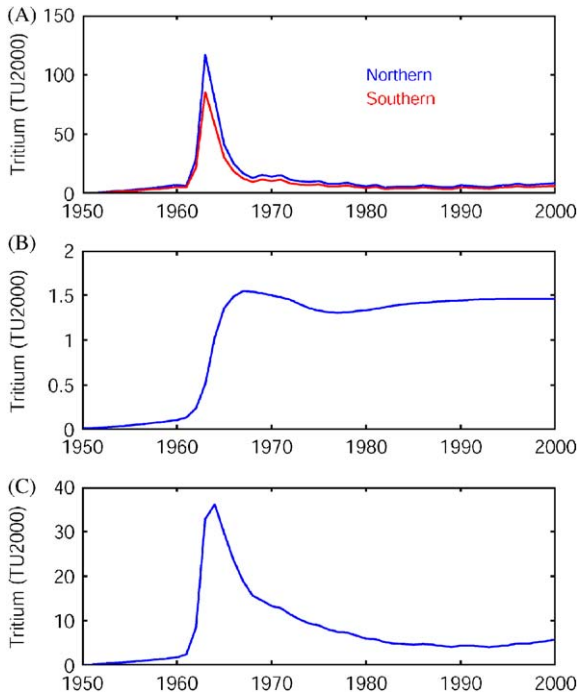


Fig. 10. Tritium concentration time histories decay corrected to January 2000 for “forcing functions” for the model as a function of year. (A) Tritium in precipitation for northern (blue) and southern (red) JES. (B) Tritium concentration for incoming waters through the Tsushima Strait. (C) Tritium concentrations for the Amur River waters entering through the Tatarskiy Strait.

convergence in the southern box associated with strait flows, upwelling, and precipitation minus evaporation. There are 10 adjustable parameters in the steady-state model formulation.

The model is formulated in *MATLAB* and integrated from nominal pre-anthropogenic tritium and ^3He concentrations in 1950 to termination in 2000. Conservation equations are constructed for tritium and ^3He using the specific set of 10 parameters, and the time step (usually a small integer number of steps per year) computed for Courant stability. The concentration of ^3He is held to zero in the surface boxes, and grows in from tritium decay. The model was run in two modes. In both modes, the mixing rates are held constant for the duration of the model integration. In the steady-state mode, the water mass formation rates are also held constant as a function of

time. In the non-steady-state mode, the water mass formation rates are held constant until a “switch year”, and then changed to new, constant values for the remainder of the integration.

4.1.2. Optimisation procedure

The tritium measurements span a nearly 15-year period (observations from 1984, 1987, 1995 and 1999 (Kaji et al., 1988; Watanabe et al., 1991; CREAMS 1995, unpublished data)) and ^3He measurements are available for a more limited time (1995 and 1999). A cost function is constructed that is the quadrature sum of uncertainty normalized model-observation differences, divided by the number of degrees of freedom.

$$\text{CF} = \frac{\sum_i \left(\frac{y_m - y_i}{\sigma_i} \right)^2}{(N - n)},$$

where y_i corresponds to a water mass observation (e.g., mean tritium concentration in the bottom water in 1995), y_m is the model simulated value, σ_i is the uncertainty in the observation, N is the number of observational constraints (32), and n is the number of parameters (10 for steady state, 14 for the non-steady state) used in the model. Observational points were obtained by averaging tritium or ^3He concentrations within a specific water mass and uncertainties estimated from statistics and/or stated analytical errors.

Constrained optimisation of the model parameterisation was achieved using a standard multi-dimensional sequential quadratic programming procedure “*fmincon*” from the *Optimization Toolbox* in *MATLAB*. Model parameters were constrained to be non-negative, and initialised to “reasonable”, non-zero values prior to optimisation. Experimentation revealed that the optimised parameter set was independent of the initial values.

4.1.3. Model results

The model was first run as a steady-state system (i.e. with exchange and water mass formation rates independent of time). The optimised cost function for the steady state simulation was 4.67, and the optimal parameters are summarized in Table 1. The optimised solution reduces all the

Table 1
Parameter results for the steady-state JES ventilation model

Parameter type	Parameter	Value ($10^{12} \text{m}^3 \text{y}^{-1}$)
Exchange	Southern : northern surface	17.5
	Northern surface : intermediate water	34.1
	Intermediate water : central water	17.9
	Central water : deep water	19.8
	Deep water: bottom water	17.8
	Southern surface: intermediate water	0
Water mass formation	Intermediate water	12.7
	Central water	0
	Deep water	0
	Bottom water	0

water mass formation rates, except for that of the Intermediate box, to zero. That is, the optimised solution achieves ventilation of the deeper boxes by a purely “diffusive” mechanism. While this seems a rather unphysical solution, it results from the fact that mixing is the only mechanism that achieves some degree of constancy of the tritium and ^3He in the three deepest boxes while accomplishing sufficient ventilation on average to reach the observed values, which is what the observations demand.

The model was then run as a non-steady-state system. Because of the rather limited time-series information, we chose the simplest mode of variation: constant exchange (mixing) rates for the duration of the integration, and a step change in water mass formation rates at one point in time during the integration. Model parameterisation was optimised for a specific choice of “switch year” (i.e. the year when the ventilation rates changed), which was systematically changed from early in the integration period to late in the period. The resultant cost function, shown in Fig. 11 was sensitive to the choice of switch year, and was a minimum value of 3.05 in 1966. Four things are evident from the cost-function behaviour shown in Fig. 11. Firstly, the cost function is significantly improved over the steady-state model, and hence demonstrates that a significant change in ventilation rates has indeed occurred. This is consistent with the historical observations discussed earlier in this paper. Secondly, the model puts significant bounds on the switch year, approximately ± 5

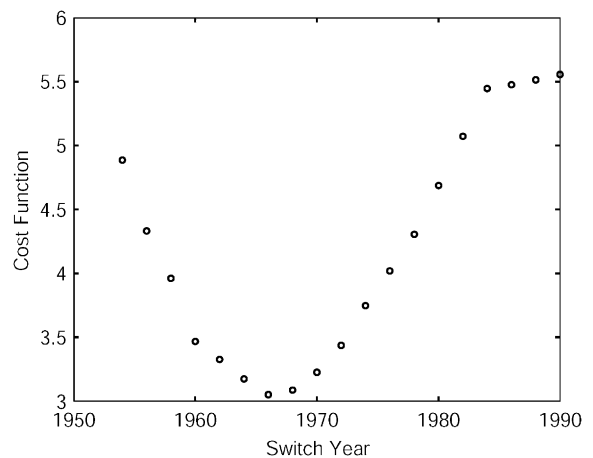


Fig. 11. Cost function vs. the year when water mass formation rates are allowed to change in the JES ventilation model.

years. This sensitivity arises from the structure of the forcing curves (see Fig. 10), since modest changes in the switch year effect rather significant changes in the integrated tritium delivery to the deeper boxes. Moreover, the respective deep box ^3He /tritium ratios become rather sensitive indicators of the timing of this delivery. The timing of the transition is consistent with the conclusions reached by Riser et al. (1999) on the basis of CFC ages in the JES. These authors found that the observed CFC ages suggested a cessation of ventilation rates in the latter half of the 1960s. Finally, extending the switch year to either extremely early or late in the integration inflates the cost function to ~ 5.5 , which is crudely

consistent with the steady-state optimum of ~ 4.7 when corrected for differences in the degrees of freedom between the two models. This “asymptotic” behaviour occurs because when the switch year occurs near the beginning or end of the integration, little time is available for accumulation of changed ventilation characteristics.

Figs. 12 and 13 compare the optimised model tritium and ^3He time series with the available data and Table 2 summarizes the optimum parameterisation for the non-steady state model run. There are two dramatic aspects of the behaviour of the model. The first is that mixing is virtually eliminated between the deep boxes. This is consistent with our current understanding of diapycnal mixing rates in the ocean (e.g., see Ledwell et al., 1993). The second is that there is an abrupt cessation of formation of intermediate, deep and bottom water in the mid-1960s. Prior to this cessation, ventilation time-scales for the intermediate, central, deep and bottom waters were approximately 4, 83, 44 and 48 years, respectively. Post 1966, there was a virtual cessation in the deep- and bottom-water formation coupled with a weak increase in central water ventilation. Intermediate waters remained ventilated by exchange, but there was a two-fold increase in residence time. The ventilation time-scales for intermediate, central, and deep waters

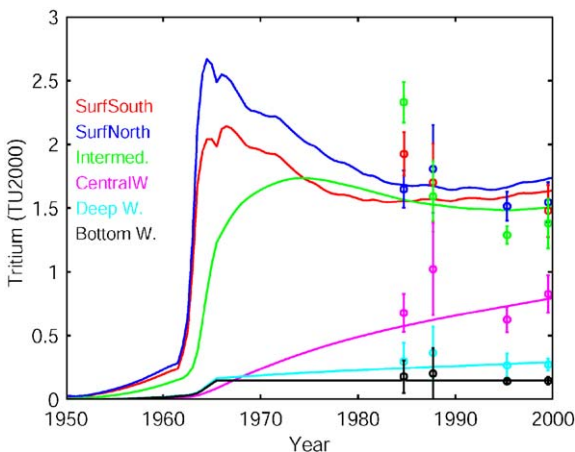


Fig. 12. JES ventilation model tritium response vs. time for the optimal case, with observations (open circles). Model tritium and observations are decay corrected to January 1, 2000.

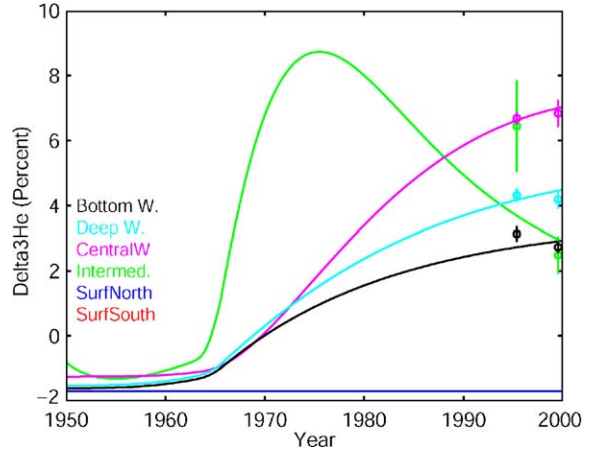


Fig. 13. JES ventilation model helium-3 response (as isotope ratio anomaly relative to air in percent) vs. time for the optimal case, with observations (open circles).

changed to 7, 64, and 450 years, while the bottom waters appear to be completely isolated.

4.2. Ventilation processes

4.2.1. Sea ice melt

A shallow salinity minimum is observed in the Japan Basin below 200 m that traces the Japan Sea Intermediate Water (JSIW) (Fig. 14). This is coupled with dissolved oxygen and CFC concentration maxima (Min, 1999) that suggest recent ventilation. Tritium maxima and $\delta^3\text{He}$ minima are present at several stations in the Japan Basin and the southern Tatarskiy Strait (values highlighted in Fig. 14) and are consistent with a ventilation timescale of just a few years for this water mass. Martin and Kawase (1998) estimate the flux of freshwater due to melting ice in the Tatarskiy Strait to be 0.14 Sv for January–April, which may contribute to the ventilation of the JSIW. Argon undersaturation in the JSIW would be enhanced due to a contribution from melt water, which may be depleted in argon due to argon rejection during ice formation (Namiot and Bukhgalter, 1965; Postlethwaite, 2002). Although a concurrent supersaturation of helium might be expected, as helium is relatively more soluble in ice, the signal is unlikely to be preserved because of the higher gas exchange rate for helium (compared to argon).

Table 2
Parameter results for the non-steady state JES ventilation model

Parameter type	Parameter	Value ($10^{12} \text{ m}^3 \text{ y}^{-1}$)	Value ($10^{12} \text{ m}^3 \text{ y}^{-1}$)
Exchange	Southern: northern surface	33.0	
	Northern surface: intermediate water	39.9	
	Intermediate water: central water	0.9	
	Central water: deep water	0	
	Deep water: bottom water	0	
	Southern surface: intermediate water	0	
Water mass formation		Pre 1966	Post 1966
	Intermediate water	35.5	0
	Central water	5.6	7.5
	Deep water	9.5	0.94
	Bottom water	5.4	0

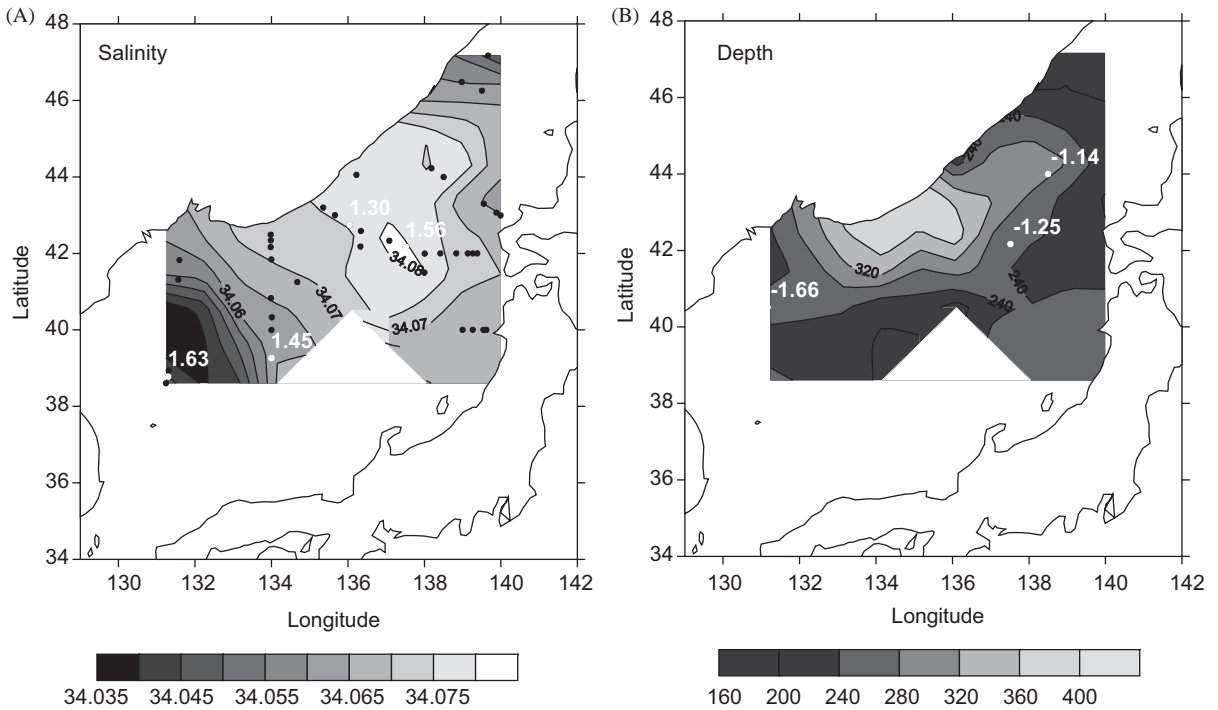


Fig. 14. Contour plot of (A) salinity and (B) depth (m) of the salinity minimum that traces the Japan Sea Intermediate Water. The tritium concentration and helium-3 isotope ratio of the corresponding tritium maximum and helium-3 minimum are labelled on the salinity and depth plots, respectively.

Sea-ice formation has minimal effect on neon, as the solubility of neon in sea ice is very similar to that in seawater (Postlethwaite, 2002). There is weak evidence of a negative correlation between salinity and argon saturation anomaly in the JSIW

(Fig. 15, $r^2 = 0.43$), which suggests that sea-ice melt may be a significant ventilation mechanism. Similar argon undersaturation was observed at the Kyodo North Pacific Ocean Time-series (KNOT—located in the Pacific about 10° east of the north

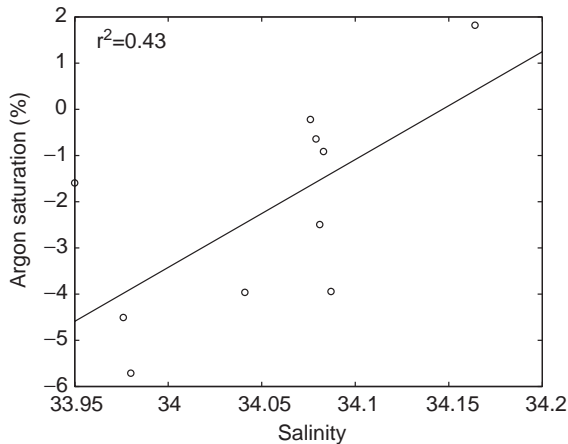


Fig. 15. Argon saturation plotted against salinity for samples from ~200 m depth. Although the correlation is weak ($r^2 = 0.43$), a saturation minimum is observed at the salinity minimum, which could be evidence of meltwater.

Hokkaido coast) in water masses affected by Sea of Okhotsk Intermediate Water that records sea-ice processes (Hamme and Emerson, 2002).

Given the spatial distribution of the salinity minimum and ^3H and ^3He extrema that trace the JSIW, we propose that this water mass may be in part ventilated by subduction of cold melt water from the north and west sectors of the JES. No evidence of this young water (i.e. a $\delta^3\text{He}$ minimum associated with the JSIW) is seen in the northern Tatarskiy Strait during the summer 1999 cruise, suggesting that this area may not be the source region for this water mass. However, such an observation cannot be conclusive, as it is conceivable that the seasonal signature of JSIW formation may be erased during spring and summer by the southward flux of the melt water via the Liman Current.

4.2.2. Convection

The range of oxygen isotope ratios observed in the subsurface water masses in the JES highlights that (at least) two deep-water formation processes are significant. The first mechanism, thermal convection, is thought to be significant close to the coast of Vladivostok where coastal topography enhances the wind field, which when combined with cold, dry continental air masses causes large

turbulent and latent heat fluxes (Kawamura and Wu, 1998). This process increases both the salinity and $\delta^{18}\text{O}$ value of the initial water mass, based on the degree of evaporation that occurs through latent heat loss. The latent heat flux comprises approximately half of the total heat loss, from the northwestern sector of the JES during the winter months ($\sim 133 \text{ W/m}^2$ Hirose et al., 1996). Sensible heat flux is the other major component of the wintertime heat loss, but this flux affects neither the salinity nor the $\delta^{18}\text{O}$ of the water mass. We use the freshwater budget and the isotopic fractionation of evaporation (Majoube, 1971) to estimate the salinity and $\delta^{18}\text{O}$ increase caused by evaporation.

Subsurface $\delta^{18}\text{O}$ values that fall on the surface $\delta^{18}\text{O}$ -Salinity Warm Mixing Line (Fig. 3) cannot be explained in terms of thermal convection of the fresher and isotopically lighter water masses originating from the north and northwestern parts of the JES, as the effect of fractionation during evaporation is insufficient to generate such values. Instead, it points to an origin to the south or east of the JES, where the $\delta^{18}\text{O}$ values are isotopically heavier. These signals could be transported via eddies of warm salty water spawned from the sub-polar front, which are cooled while propagating north/westwards (e.g. Nishiyama et al., 1993). Alternatively, these data may support the results of Aubrey et al. (2000), who discuss a belt of warm water moving along 42°N from Hokkaido towards the west during the winter, forming deep water as it cools on the way. Such a westward-moving water mass would indeed be isotopically heavy (Station 88 near the coast of Hokkaido at around 42°N has a mean $\delta^{18}\text{O}$ value of $0.13 \pm 0.08\text{‰}$). Certainly, cooling of waters originating from south of the sub-polar front is the significant water mass formation mechanism for these data.

The negative subsurface $\delta^{18}\text{O}$ values cannot have originated from thermal convection in the northern part of the sea, as the salinity is too low in those regions (Seung and Yoon, 1995). The negative $\delta^{18}\text{O}$ values could, however, have originated by the second deep-water formation mechanism, brine rejection, in the northern sector of the JES, as this process simultaneously increases salinity and decreases $\delta^{18}\text{O}$ in the seawater

(Macdonald et al., 1995). The very lightest subsurface $\delta^{18}\text{O}$ values are thought to originate from brine rejection during freezing in regions of substantially freshwater diluted surface waters, e.g. in coastal regions near the Liman Current.

To determine the influence of sea-ice formation in the Tatarskiy Strait and Peter the Great Bay on dense-water formation in the JES, we calculate the fraction of the mixed layer that would need to be frozen in order to alter the salinity, $\delta^{18}\text{O}$ and argon to those observed in bottom water by brine rejection. Conservation of salt (S), oxygen isotopes ($\delta^{18}\text{O}$), argon (A) and helium (H) requires

$$S_0 = S_i f + S_{\text{BW}}(1 - f), \quad (1)$$

$$\delta^{18}\text{O}_0 = (\delta^{18}\text{O}_i + \alpha)f + \delta^{18}\text{O}_{\text{BW}}(1 - f), \quad (2)$$

$$A_0 = A_i f + A_{\text{BW}}(1 - f), \quad (3)$$

$$H_0 = H_i f + H_{\text{BW}}(1 - f), \quad (4)$$

where f is the fraction of the mixed layer taken up as sea ice, α is the isotopic increase caused by fractionation during sea ice formation (2.57‰; Macdonald et al., 1995), and the subscripts 0, i and BW correspond to the original unfrozen mixed layer, the sea ice and the newly formed bottom water, respectively. Here gas exchange is assumed to be negligible in the conservation of argon and helium due to the presence of the ice barrier and rapid convection away from the surface.

Very few measurements of wintertime pre-ice salinity in the Tatarskiy Strait are available, and we therefore treat it as an unknown. The salinity of the sea ice (S_i) was estimated as $0.31 \cdot S_0$ (Martin and Kaufman, 1981). Although this is likely an overestimation of the final salinity of the sea ice, it provides an upper bound for the amount of ice formed and is thus a useful estimate. A salinity of 34.067 and oxygen isotope value of 0.03‰ are used for the bottom water (S_{BW} and $\delta^{18}\text{O}_{\text{BW}}$), i.e. the average of all CREAMS 1999 samples taken below 2500 m. $\delta^{18}\text{O}_0$ is taken as a function of the unknown S_0 from the linear regression of the surface $\delta^{18}\text{O}$ on salinity ($\delta^{18}\text{O}_0 = 0.60 \times S_0 - 20.31$, Cold Mixing Line, Fig. 3). Substituting

and rearranging Eqs. (1) and (2) gives

$$S_0 = \frac{S_{\text{BW}}(1 - f)}{(1 - 0.31f)}, \quad (5)$$

$$0.60 \times S_0 - 20.31 = \delta^{18}\text{O}_{\text{BW}} + \frac{\alpha f}{(1 - f)}. \quad (6)$$

Eqs. (5) and (6) are solved simultaneously to give $f = 0.006$ and $S_0 = 33.929$ and hence $\delta^{18}\text{O}_0 = 0.05\%$. The decrease in $\delta^{18}\text{O}$ from pre-ice to ice-covered conditions is not discernible within the accuracy of the measurements and is plotted in Fig. 3 (open diamonds and solid line). Obviously the calculated changes are not sufficient to explain the very lightest oxygen isotope measurements observed in the western Japan Basin but these extreme values may result from regionally more intense brine rejection events, or episodes of multiple freeze-thaw cycles that may have been more frequent in the past. Indeed, substituting the lightest observed $\delta^{18}\text{O}$ data from the deep water (-0.25%) in the calculations discussed above suggests that 2% of the mixed layer is required to freeze, with the initial water having a salinity of 33.53 and an oxygen isotope ratio of -0.19% (open squares and solid line, Fig. 3). Parkinson et al. (1999) discuss a decrease of 20% sea-ice extent per decade since 1978 in the JES and Sea of Okhotsk, which supports this hypothesis.

The fraction of the mixed layer that is thought to freeze based on the salinity and oxygen isotope distributions (f) can be substituted into Eqs. (3) and (4), in order to infer the changes in argon and helium concentration caused by this amount of sea-ice formation. We use $A_i = 0.08 \times A_0$ and $H_i = 1.12 \times H_0$ as an estimate of the amount of argon and helium in sea ice (Postlethwaite, 2002). This takes into account that argon is almost completely insoluble in sea ice and helium is slightly more soluble in sea ice than it is in seawater. A_{BW} and H_{BW} , the argon and helium concentration of the newly formed bottom water, are taken as the mean argon and helium concentrations of the water mass beneath 2500 m that are not affected by air injection ($A_{\text{BW}} = 3.677 \pm 0.025 \times 10^{-4} \text{ cm}^3(\text{STP})/\text{g}$, $H_{\text{BW}} = 4.144 \pm 0.027 \times 10^{-8} \text{ cm}^3(\text{STP})/\text{g}$). Based on these conditions, the initial argon and helium concentrations are

estimated to be $A_0 = 3.657 \times 10^{-4} \text{ cm}^3(\text{STP})/\text{g}$ and $H_0 = 4.147 \times 10^{-8} \text{ cm}^3(\text{STP})/\text{g}$, which would imply that the water mass was undersaturated in argon by $\sim 8\%$ and supersaturated by $\sim 3\%$ in helium prior to freezing. The increase in argon concentration and decrease in helium concentration brought about by this amount of ice production is not significant within the analytical precision that applies to the data. Freezing 2% of the mixed layer would lead to a significant change in argon concentration (open squares and solid line in Fig. 6) and may explain the deviation from the two main mixing lines seen in subsurface water masses in the JES (Fig. 6). We hypothesize that the source of the concurrent dissolved argon increase and dissolved helium decrease seen in a subset of samples from the western Japan Basin and western Tatarskiy Strait is rapid freezing of a large fraction of the water column ($> 5\%$, Fig. 6) in regions of substantial freshwater influence.

Prior to ice formation, the mixed layer in the Tatarskiy Strait is approximately 100 m thick, based on temperature and salinity profiles taken during December 1999 from PALACE float 194 in the southern Tatarskiy Strait (Riser, 1999). The salinity budget calculation above, implies that a fraction $f = 0.006 \pm 0.004$ of the mixed layer was required to freeze, in order to generate the mean surface to bottom-water salinity and $\delta^{18}\text{O}$ differences that were observed, giving a mean ice thickness of approximately $0.6 \pm 0.4 \text{ m}$, which is within the range of ice thickness observations from the region reported in Martin et al. (1992) (0.5–1.5 m). The volume of bottom-water formed due to this amount of ice formation can be estimated as $V_{\text{BW}} = (1 - f) \times V_{\text{ML}}$, where V_{ML} , the volume of the mixed layer, is taken to be the area of the Tatarskiy Strait covered by sea ice ($4 \times 10^{10} \text{ m}^2$, Martin et al., 1992) multiplied by the mixed-layer depth, giving $V_{\text{BW}} = 3.97 \pm 0.89 \times 10^{12} \text{ m}^3$. Based on the bottom-water formation rate estimated from the switchover box model discussed earlier ($5.4 \times 10^{12} \text{ m}^3 \text{ yr}^{-1}$ prior to the mid-1960s), brine rejection could have accounted for between 60–90% of the bottom-water formed per year. Despite the large errors associated with this estimate, V_{BW} is significantly larger than the volume of bottom-water formed due to sea-ice

formation estimated by Martin et al. (1992) ($0.4\text{--}1.2 \times 10^{12} \text{ m}^3$). Differences between our estimate of V_{BW} and that of Martin et al. (1992) arise predominantly from differences in the salinity of the seawater prior to ice formation. Martin et al. (1992) use summertime salinity measurements from the region, when the influence of the Amur and other rivers are significant in lowering the surface salinity in the Tatarskiy Strait, to estimate the pre-ice salinity. This could lead to a serious underestimation in the salt flux from forming ice. Caution is required when interpreting our rather large estimate of the volume of bottom-water formed due to sea-ice formation, as we have assumed that brine rejection only contributes to the ventilation of the bottom water, whereas in reality, sea-ice formation is likely to influence all of the subsurface water masses, thereby decreasing the overall impact to the bottom water.

5. Summary and conclusions

A potential explanation of the tracer observations in the JES is outlined in Fig. 16. A wide range of oxygen isotope ratios in the JES proper water indicates at least two significant ventilation mechanisms; (a) convection through cooling of water masses from south of the sub-polar front, and (b) convection through sea-ice formation and brine rejection in the north and west of the JES. $\delta^{18}\text{O}$ is most negative in the north western Japan Basin, indicating that this region is likely influenced by sea-ice formation and brine rejection. Sea-ice formation and the subsequent brine rejection from freezing seawater with the properties of the surface water observed in the northern Tatarskiy Strait and western Japan Basin during the summer 1999 CREAMS cruises would not be sufficient to generate the lowest $\delta^{18}\text{O}$ values or highest argon concentrations seen in the subsurface waters in the northern and northwestern JES. Brine rejection must have been more extensive in the past in order to explain these observations.

Assuming that the salinity of the bottom water in the JES has not changed since that time, increased brine rejection implies that the pre-ice surface salinity in the ice formation region must

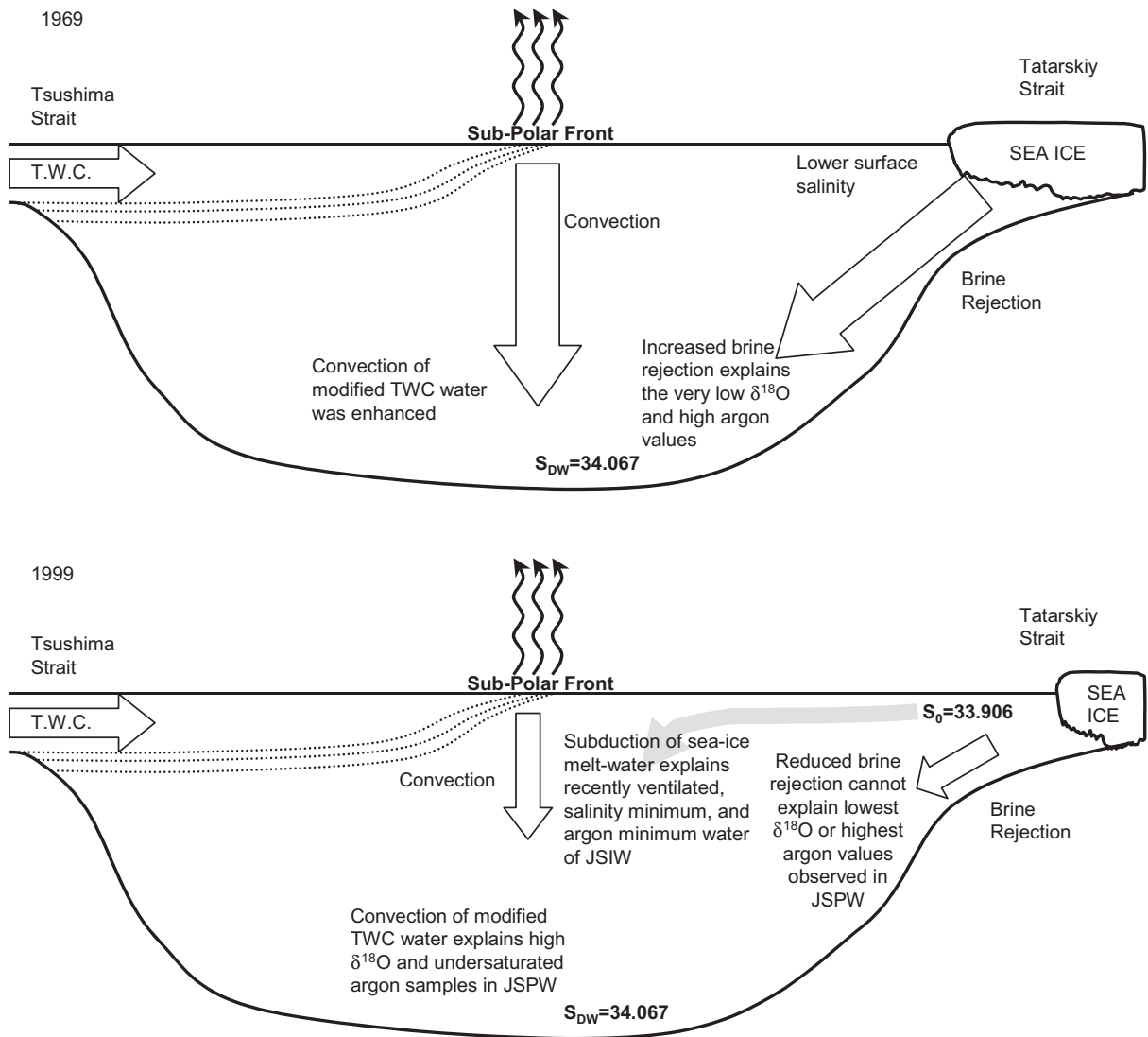


Fig. 16. Schematic of the water mass ventilation in the JES in 1969 and 1999 inferred from the tracer data.

have been lower. Interestingly, during the 1950s when changes to the deep and bottom waters in the JES are thought to have started (Gamo et al., 1986), the number of dams commissioned in China increased dramatically. If this change to the number of dams during the 1950s decreased the freshwater input to the Japan Sea, the argument of Nof (2001) may imply an increase in thermally driven convection since that time. Increasing the surface salinity would moreover depress the

freezing point of seawater, making ice formation more difficult. So the net effect of decreasing freshwater input could be a combination of increased thermal convection and decreased sea-ice formation. However, the surface waters have been increasing in temperature over the same time period (Kim et al., 2001), which may counteract any effects of enhanced thermal convection due to a decrease in freshwater input, and would further inhibit ice formation.

Tritium and $\delta^3\text{He}$ results may show that deep-water formation processes have been sharply reduced since the 1960s, suggesting that brine rejection in the Tatarskiy Strait is not currently a significant deep-water formation mechanism in the JES. However, the model calculations suggest that JSIW is still being formed, albeit at reduced rates, and that sea-ice melt water may be a significant ventilation mechanism for the JSIW based on an argon minimum at the recently ventilated salinity minimum in the Tatarskiy Strait and Western Japan Basins.

In the intermediate and central waters, there are basin-wide differences between tritium distribution on isopycnals, with the highest found in the western Japan Basin and the lowest found in the Yamato Basin and the Tatarskiy Strait. This indicates that these water masses are more recently ventilated in the western Japan Basin and then spread to the Ulleung Basin and finally to the Yamato Basin. The tritium concentration in the deep and bottom waters of the JES is remarkably similar throughout all three main basins. However, differences exist in the $\delta^3\text{He}$ values for the different regions of the JES indicating differences in age. The Ulleung Basin has $\sim 1\%$ higher $\delta^3\text{He}$ values than the other regions of the JES for the water mass centered on $\sigma_2 = 36.67$, indicating older water. This is consistent with Min and Warner (2005) who found the lowest CFC's for Japan Sea Deep Water in the Ulleung and Yamato Basins.

A 6-box model of the JES calibrated with tritium and ^3He observations performed significantly better when there was a significant reduction of subsurface water mass formation rates in the mid-1960s. Model central-, deep- and bottom-water production rates prior to this cessation were 5.6, 9.5, and $5.4 \times 10^{12} \text{m}^3 \text{yr}^{-1}$ respectively. Post-cessation rates were 7.5, 0.9, and $0 \times 10^{12} \text{m}^3 \text{yr}^{-1}$, respectively. The salinity and oxygen isotope budgets implied a potential bottom water formation rate of $3.97 \pm 0.89 \times 10^{12} \text{m}^3 \text{yr}^{-1}$ from sea-ice production. Thus, it could be argued that brine-rejection processes could account for somewhere between 20% and 50% of the total subsurface water production (excluding JSIW). Inasmuch as the salinity and oxygen isotopes are fundamentally integrative, we conclude that they indicate that brine rejection accounts for a time-average fraction of the

ventilation process corresponding to between 25% and 35% of subsurface water formation in the JES.

Acknowledgements

This work was funded by the Natural Environment Research Council projects GR3/11980 and GR9/04548. We express our thanks to Lynne Talley, Vladimir Luchin and the scientists, officers and crew of the R.V.s *Roger Revelle* and *Professor Khromov*. Thanks to Clementine Griveaud who contributed to the oxygen isotope analyses as part of her SOCRATES exchange project.

References

- Aubrey, D.G., Danchenkov, M.A., Riser, S.C., 2000. Belt of salt water in the north-western Japan Sea. In: Danchenkov, M.A. (Ed.), CREAMS International Symposium, Vladivostok, pp. 11–20.
- Benson, B., Kraus, D., 1980. Isotopic fractionation of helium during solution: a probe for the liquid state. *Journal of Solution Chemistry* 9, 895–909.
- Broecker, W.S., Peng, T.H., Östlund, G., 1986. The distribution of bomb tritium in the ocean. *Journal of Geophysical Research* 91, 14331–14344.
- Clarke, W.B., Jenkins, W.J., Top, Z., 1976. Determination of tritium by mass spectrometric measurement of ^3He . *International Journal of Applied Radiation and Isotopes* 27, 515–522.
- Doney, S., Jenkins, W., Ostlund, H., 1993. A tritium budget for the North Atlantic. *Journal of Geophysical Research* 98, 18069–18081.
- Gamo, T., Horibe, Y., 1983. Abyssal circulation in the Japan Sea. *Journal of the Oceanographical Society of Japan* 39, 220–230.
- Gamo, T., Nozaki, Y., Sakai, H., Nakai, T., Tsubota, H., 1986. Spatial and temporal variations of water characteristics in the Japan Sea bottom layers. *Journal of Marine Research* 44, 781–793.
- Hamme, R., Emerson, S., 2002. Mechanisms controlling the global oceanic distribution of the inert gases argon, nitrogen and neon. *Geophysical Research Letters* 29, 2120, doi:10.1029/2002GL015273.
- Harada, K., Tsunogai, S., 1986. ^{226}Ra in the Japan Sea and the residence time of the Japan Sea water. *Earth and Planetary Science Letters* 77, 236–244.
- Hirose, N., Kim, C.-H., Yoon, J.-H., 1996. Heat budget in the Japan Sea. *Journal of Oceanography* 52, 553–574.
- Hood, E.M., Howes, B.L., Jenkins, W.J., 1998. Dissolved gas dynamics in perennially ice-covered Lake Fryxell, Antarctica. *Limnology and Oceanography* 43, 265–272.

- Josey, S., Kent, E., Taylor, P., 1999. New insights into the ocean budget closure problem from the analysis of the SOC air-sea flux climatology. *Journal of Climate* 12, 2846–2888.
- Kaji, T., Momoshima, N., Takashima, Y., 1988. Tritium concentrations of the deep sea-water in the Japan Sea and the Pacific Ocean. *Journal of Radioanalytical Nuclear Chemistry Letters* 127, 447–456.
- Kawamura, H., Wu, P., 1998. Formation mechanism of Japan Sea Proper Water in the flux center off Vladivostok. *Journal of Geophysical Research* 103, 21611–21622.
- Keeling, R.F., 1993. On the role of large bubbles in air-sea gas exchange and supersaturation in the ocean. *Journal of Marine Research* 51, 237–271.
- Kim, K., Kim, K.-R., Min, D.-H., Volkov, Y., Yoon, J.-H., Takematsu, M., 2001. Warming and structural changes in the East (Japan) Sea: a clue to future changes in global oceans? *Geophysical Research Letters* 28, 3293–3296.
- Kim, K.R., 1997. The East Sea (Japan Sea): a miniature test ground for global changes. Recent chemical observations from CREAMS 93–96. In: Tsunogai, S. (Ed.), *Biogeochemical Processes in the North Pacific*. Japan Marine Science Foundation, pp. 41–51.
- Kim, K.R., Kim, K., 1996. What is happening in the East Sea (Japan Sea)? Recent chemical observations during CREAMS 93–96. *The Journal of the Korean Society of Oceanography* 31, 164–172.
- Kim, K.R., Kim, G., Kim, K., Lobanov, V., Pomarev, V., 2002. A sudden bottom-water formation during the severe winter 2000–2001: The case of the East/Japan Sea. *Geophysical Research Letters* 29, 1234, doi:10.1029/2001GL014498.
- Kumamoto, Y., Yoneda, M., Shibata, Y., Kume, H., Tanaka, A., Uehiro, T., Morita, M., Shitashima, K., 1998. Direct observation of the rapid turnover of the Japan Sea bottom water by means of AMS radiocarbon measurement. *Geophysical Research Letters* 25, 651–654.
- Ledwell, J.R., Watson, A.J., Law, C.S., 1993. Evidence for slow mixing rates across the pycnocline from an open-ocean tracer-release experiment. *Nature* 364, 701–703.
- Lott, D.E., Jenkins, W.J., 1984. An automated cryogenic charcoal trap system for helium isotope mass spectrometry. *Review of Scientific Instruments* 55, 1982–1988.
- Macdonald, R.W., Paton, D.W., Carmack, E.C., 1995. The freshwater budget and under-ice spreading of Mackenzie River water in the Canadian Beaufort Sea based on salinity and $^{18}\text{O}/^{16}\text{O}$ measurements in water and ice. *Journal of Geophysical Research* 100, 895–909.
- Majoube, M., 1971. Fractionnement en oxygene 18 et en deuterium entre l'eau et sa vapeur. *Journal of Chemical Physics* 10, 1423–1436.
- Martin, S., Kaufman, P., 1981. A field and laboratory study of wave damping by grease ice. *Journal of Glaciology* 27, 283–313.
- Martin, S., Kawase, M., 1998. The southern flux of sea ice in the Tatarskiy Strait, Japan Sea and the generation of the Liman Current. *Journal of Marine Research* 56, 141–155.
- Martin, S., Munoz, E., Drucker, R., 1992. The effect of severe storms on the ice cover of the northern Tatarskiy Strait. *Journal of Geophysical Research* 97, 17753–17764.
- Menard, H.W., Smith, S.M., 1966. Hypsometry of ocean basin provinces. *Journal of Geophysical Research* 71, 4305–4325.
- Min, D.H., 1999. Studies of large-scale intermediate and deep water circulation and ventilation in the North Atlantic, South Indian and Northeast Pacific Oceans, and in the East Sea (Sea of Japan), using chlorofluorocarbons as tracers. Ph.D. Thesis, University of California, San Diego.
- Min, D.H., Warner, M.J., 2005. Basin-wide circulation and ventilation study in the East Sea (Sea of Japan) using chlorofluorocarbon tracers. *Deep-Sea Research II*, in press [doi:10.1016/j.dsr2.2003.11.003].
- Namiot, A., Bukhgalter, É., 1965. Clathrates formed by gases in ice. *Journal of Structural Chemistry* 6, 911–912.
- Nishiyama, K., Inagawa, M., Mizuno, T., 1993. The Japan Sea Proper Water and water circulation in the Japan Sea. *Papers in Meteorology and Geophysics*, Tokyo 44, 1–10.
- Nof, 2001. China's development could lead to bottom water formation in the Japan/East Sea. *Bulletin of the American Meteorological Society* 82, 609–618.
- Parkinson, C.L., Cavalieri, D.J., Gloersen, P., Zwally, H.J., Comiso, J.C., 1999. Arctic sea ice extents, areas and trends 1978–1996. *Journal of Geophysical Research* 104, 20837–20856.
- Postlethwaite, C., 2002. Developing a tool for evaluating the role of seasonal sea ice in deep-water formation. Ph.D. Thesis, University of Southampton, UK.
- Riser, S., 1999. UW Japan/East Sea PALACE Floats. WWW Page, <http://flux.ocean.washington.edu/japan-sea/homographs/TP/194.html>
- Riser, S.C., Warner, M.J., Yurasov, G.I., 1999. Circulation and mixing of water masses of Tatar Strait and the northwestern boundary region of the Japan Sea. *Journal of Oceanography* 55, 133–156.
- Seung, Y., Yoon, J., 1995. Some features of winter convection in the Japan Sea. *Journal of Oceanography* 51, 61–73.
- Spitzer, W.S., Jenkins, W.J., 1989. Rates of vertical mixing, gas exchange and new production: estimates from seasonal gas cycles in the upper ocean near Bermuda. *Journal of Marine Research* 47, 169–196.
- Stark, S., Jenkins, W.J., Doney, S.C., 2004. Deposition and recirculation of tritium in the North Pacific Ocean. *Journal of Geophysical Research* 109, doi:10.1029/2003JC002150.
- Talley, L., Lobanov, V., Pomarev, V., Salyuk, A., Tishchenko, P., Zhabin, I., Riser, S., 2003. Deep convection and brine rejection in the Japan Sea. *Geophysical Research Letters* 30, 1159, doi:10.1029/2002GL016451.
- Wallace, D.W.R., Wirick, C.D., 1992. Large air-sea gas fluxes associated with breaking waves. *Nature* 356, 694–696.
- Watanabe, Y.W., Watanabe, S., Tsunogai, S., 1991. Tritium in the Japan Sea and the renewal time of the Japan Sea Deep Water. *Marine Chemistry* 34, 97–108.
- Yamamoto, M., Tanaka, N., Tsunogai, S., 2001. Okhotsk Sea intermediate water formation deduced from oxygen isotope systematics. *Journal of Geophysical Research* 106, 31,075–31,084.